View metadata, citation and similar papers at core.ac.uk
brought to you by CORE
provided by Missouri University of Science and Technology (Missouri S&T): Scholars' Mine

Missouri University of Science and Technology
Scholars' Mine

Physics Faculty Research & Creative Works | Physics

01 Jan 2014

Kapitza Resistance of Si/SiO_2 Interface

Bowen Deng

Aleksandr V. Chernatynskiy
Missouri University of Science and Technology, aleksandrc@mst.edu

Marat Khafizov

David H. Hurley

et. al. For a complete list of authors, see https://scholarsmine.mst.edu/phys_facwork/469

Follow this and additional works at: https://scholarsmine.mst.edu/phys_facwork

Part of the Numerical Analysis and Scientific Computing Commons, and the Physics Commons

Recommended Citation

B. Deng et al., "Kapitza Resistance of Si/SiO_2 Interface," *Journal of Applied Physics*, vol. 115, no. 8, American Institute of Physics (AIP), Jan 2014.
The definitive version is available at https://doi.org/10.1063/1.4867047

This Article - Journal is brought to you for free and open access by Scholars' Mine. It has been accepted for inclusion in Physics Faculty Research & Creative Works by an authorized administrator of Scholars' Mine. This work is protected by U. S. Copyright Law. Unauthorized use including reproduction for redistribution requires the permission of the copyright holder. For more information, please contact scholarsmine@mst.edu.

JOURNAL OF APPLIED PHYSICS 115, 084910 (2014)

Kapitza resistance of Si/SiO_2 interface

B. Deng (邓博文),[1] A. Chernatynskiy,[1] M. Khafizov,[2] D. H. Hurley,[2] and S. R. Phillpot[1,a)]
[1]*Department of Materials Science and Engineering, University of Florida, Gainesville, Florida 32611, USA*
[2]*Department of Materials Science and Engineering, Idaho National Laboratory, Idaho Falls, Idaho 83415, USA*

(Received 8 January 2014; accepted 16 February 2014; published online 27 February 2014)

A phonon wave packet dynamics method is used to characterize the Kapitza resistance of a Si/SiO_2 interface in a $Si/SiO_2/Si$ heterostructure. By varying the thickness of SiO_2 layer sandwiched between two Si layers, we determine the Kapitza resistance for the Si/SiO_2 interface from both wave packet dynamics and a direct, non-equilibrium molecular dynamics approach. The good agreement between the two methods indicates that they have each captured the anharmonic phonon scatterings at the interface. Moreover, detailed analysis provides insights as to how individual phonon mode scatters at the interface and their contribution to the Kapitza resistance.
© *2014 AIP Publishing LLC*. [http://dx.doi.org/10.1063/1.4867047]

I. INTRODUCTION

The Kapitza resistance is the thermal boundary resistance presented at the interface between two blocks of materials. This resistance has two basic origins: the structural disorder associated with the interface and the different properties of the heat carriers on the two sides of the interface. One or other of the mechanisms is operative at all interfaces; both are present at some interfaces.

In the case of electrical insulators, including most ionically bonded systems and many semiconductors, the dominant heat carriers are phonons. As a result, the Kapitza resistance is governed by details of the interfacial structure and the availability of vibrational states on the two sides of the interface. The Kapitza resistance is critical in the silicon on insulator (SOI) technology in microelectronics, where SiO_2 has long been used as a dielectric. The SOI wafer structure is normally made up of a thin layer of insulating materials (typically SiO_2) separating single crystalline Si.[1] However, the overall cooling of the electronics by thermal conduction can be limited by both the introduction of the low thermal conduction oxide layer and the Si/SiO_2 interfaces themselves. Previously, Hurley *et al.* have measured the Kapitza resistance across a bicrystal interface of silicon.[2] Using high resolution transmission electron microscopy, they found a native 4.5 nm thick SiO_2 layer was present at the interface; they estimated the Si/SiO_2 boundary resistance by comparing experimental results with a continuum thermal transport model.

There have been previous molecular dynamics (MD) simulations of the Kapitza resistance of Si/SiO_2 interfaces. Mahajan *et al.*[3] estimated the Kapitza resistance to be $\sim 0.5 \times 10^{-9}$ Km^2W^{-1} using an extended Stillinger-Weber (SW) potential. Lampin *et al.*[4] calculated the Si/SiO_2 boundary resistance to be 0.4×10^{-9} Km^2W^{-1} at 500 K with the Tersoff potential[5] using the "approach-to-equilibrium molecular dynamics" (AEMD) method. They found that this boundary resistance is large enough to change the heat properties in the case of ultra-thin buried oxide layers. Chen *et al.*[6] focused on how the strength of the coupling across the interface affects the Si/SiO_2 interface resistance using non-equilibrium molecular dynamics (NEMD). They found that in the weak interfacial coupling limit, the boundary resistance is sensitive to the details of the interfacial structure; in the strong coupling limit the boundary resistance is not sensitive to the details of the interface structure. In this strong coupling limit, the Si/SiO_2 boundary resistance was found to be 0.9×10^{-9} Km^2W^{-1}. While all of these theoretical estimates give broad agreement as to the magnitude of the Kapitza resistance, they do not provide any insights as to which branches and wavelengths of phonons are involved.

In this study, we characterize the scattering of phonons at the Si/SiO_2 interface using the phonon wave-packet dynamics (PWD) technique. This approach has been extensively used in the study of phonon scatterings in various silicon microstructures.[7–9] We also use the NEMD method to determine the thermal resistance of the interface. While most of the previous studies focused on the role of intrinsic and extrinsic defects in silicon,[7–9] here, we concentrate on a detailed description of the phonon scattering at the Si/SiO_2 interface. The rest of the paper is organized as follows: Sec. II describes the simulation and analytical approaches we use; Section III focus on the simulation results and their analysis to characterize the energy transmission coefficient, phonon-interface scattering events, mode conversion, and Kapitza resistance calculation. Our conclusions are in Sec. IV.

II. SIMULATION METHOD

To investigate the thermal transport at the Si/SiO_2 interface, we set up our structure in a manner analogous to the experiment,[2] where a thin layer of SiO_2 film is sandwiched between two blocks of Si crystal. Here, the two Si crystals have the same crystallographic orientation. This differs from the experimental situation of Hurley *et al.* in which the two Si crystals form a twist grain boundary. However, as we shall see, due to the presence of the SiO_2 layer, the presence or

[a)]Author to whom correspondence should be addressed. Electronic mail: sphil@mse.ufl.edu

 © 2014 AIP Publishing LLC

absence of a misorientation between the two Si crystals does not affect phonon dynamics; moreover, our structure allows smaller cross sections to be used, which has a significantly lower computational load. The simulation setups for the wave-packet dynamics and NEMD simulations are sketched in Figure 1. Note that the silicon crystals are extremely long in the structure used for wave-packet dynamics so that we can fully analyze the transmitted and reflected wave packets.

To build the sandwich structure, the blocks of crystalline Si are fully quenched to very low forces and stresses; the lattice constant in the cross-sectional directions during annealing is fixed to its bulk value. The SiO_2 is prepared initially as β-cristobalite and strained (about 1%) in order to fit the Si lattices in the (001) plane. The structure used for PWD simulations has 4×4 silicon unit cells in the (001) cross-sectional plane and is about 1600 nm long. Various thicknesses of the SiO_2 layer, from 0.8 to 24 nm are used. We chose the relatively small 4×4 cross-sectional area of Si to limit the computational power needed for a systems of such great length. The β-cristobalite SiO_2, a high temperature phase, was chosen for the initial structure of the oxide layer due to smallest mismatch with the Si lattice. However, we do not expect that this particular choice of the initial SiO_2 crystal structure to is very important since the very thin oxide layers considered here undergo partial amorphization upon annealing. The entire system is then annealed, which includes heating to 2000 K to enable bonding at the interfaces and a rigorous final quenching, so that all of the forces are very small, less than 10^{-7} eV/Å per atom. This eliminates any excess structural energy that could affect the phonon scattering simulations. The same approach is applied in preparing the structure used for the NEMD simulations, only with much shorter Si blocks (about 50 nm).

We choose the extended Stillinger-Weber potential developed by Watanabe *et al.*[10] to describe the interatomic interactions. This potential has proven capable of describing the Si/SiO_2 interface as well as its formation.[11,12] In the extended SW potential, the interaction function between Si atoms is exactly the same as the original SW potential for pure Si.[13] As shown by the silicon phonon dispersion curve in Figure 2, determined by lattice dynamics calculations, the SW potential gives reasonably good representation of the LA mode. We note that it is unable to reproduce the flatness of TA mode near the band edge due to the short-range interatomic interactions. However, as will be shown later, the energy transmission coefficient for higher frequencies (>6 THz) phonons is almost frequency independent; thus, we believe this aspect of the dispersion curve will not significantly affect our results. Further, the poor descriptions of the two optical modes (LO and TO) is not crucial to our work because they are thought not to be significant carriers of heat in Si,[14] a conclusion we confirm in our simulations.

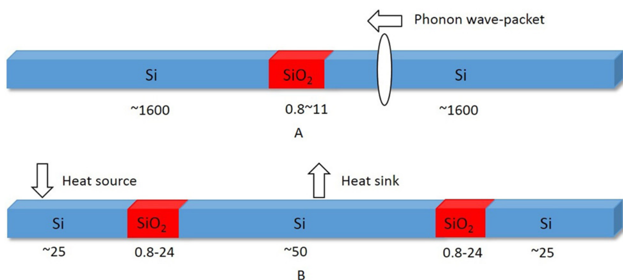

FIG. 1. Simulation setup for (A) wave-packet dynamics simulation; (B) Non-equilibrium molecular dynamics simulation. The numbers in the figure indicate the length of each block and are in the unit of nm.

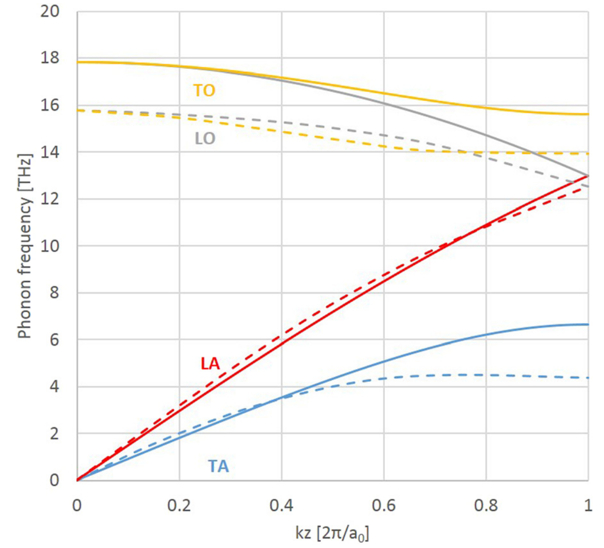

FIG. 2. Phonon dispersion relation of silicon along [001]. Solid lines are calculated from Stillinger-Weber potential from lattice dynamics using GULP;[15] dashed lines are reproduced from experiment.[16]

The core idea of PWD is to form a wave packet of phonons from a single branch with the frequency being a narrow Gaussian distribution.[8] The wave packet is generated as previously described,[8] so that it is localized in both real space and reciprocal space and with the k_z direction corresponding to [001] direction. The initial atomic displacement is generated according to Eq. (1), and a subsequent inverse discrete Fourier transformation is used to obtain the normal coordinates $a_{\lambda \mathbf{k}}$ from Eq. (2)

$$\mathbf{u}_{il} = \frac{A}{\sqrt{m}} \boldsymbol{\varepsilon}_{i\lambda\mathbf{k}_0} \exp[i\mathbf{k}_0 \cdot (\mathbf{R}_l - \mathbf{R}_0)] \exp\left[-\frac{(\mathbf{R}_l - \mathbf{R}_0)^2}{\eta^2}\right], \quad (1)$$

$$a_{\lambda\mathbf{k}} = \sqrt{\frac{m}{N}} \sum_{il} \mathbf{u}_{il} \cdot \boldsymbol{\varepsilon}^*_{i\lambda\mathbf{k}} \exp(-i\mathbf{k} \cdot \mathbf{R}_l), \quad (2)$$

where A controls the amplitude of the wave-packet and η controls the width of the wave-packet; R_0 is the center of the wave-packet, $\mathbf{u}_{il}$ and $\mathbf{R}_l$ denote the displacement vector of the *i*-th atom in *l*-th primitive cell and the coordinates of the *l*-th primitive cell. *N* is the total number of primitive cell and *m* is the mass of atom *i*. $a_{\lambda\mathbf{k}}$ is the amplitude of the phonon with wave vector $\mathbf{k}$ and branch λ, and $\boldsymbol{\varepsilon}_{i\lambda\mathbf{k}}$ and $\boldsymbol{\varepsilon}^*_{i\lambda\mathbf{k}}$ are the corresponding eigenvector and its complex conjugate for atom i, respectively. An alternative way to obtain the initial displacement is through the normal coordinates

$$\mathbf{u}_{il} = \frac{1}{\sqrt{Nm_i}} \sum_{\lambda\mathbf{k}} a_{\lambda\mathbf{k}} \boldsymbol{\varepsilon}_{i\lambda\mathbf{k}} \exp(i\mathbf{k} \cdot \mathbf{R}_l). \quad (3)$$

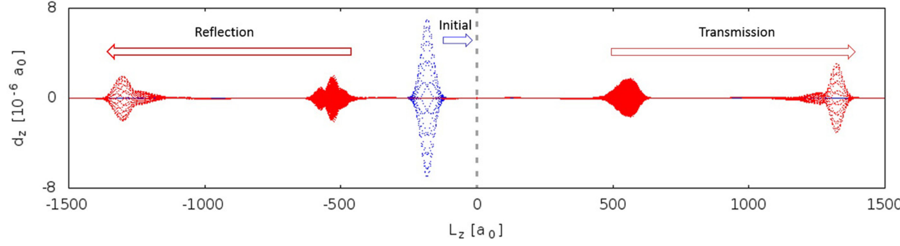

FIG. 3. Illustration of a scattering event. The vertical axis is the atomic displacement along z axis; the horizontal axis indicates the z coordination of the structure. The silica layer is located at around $L_z = 0$ (dash line) and, in this simulation, is only about $0.14a_0$ (0.8 nm) thick, where a_0 is the lattice constant of Si.

The initial velocity, $\mathbf{v}_{il}$, can then be written as

$$\mathbf{v}_{il} = \frac{1}{\sqrt{Nm_i}} \sum_{\lambda\mathbf{k}} a_{\lambda\mathbf{k}} \boldsymbol{\varepsilon}_{i\lambda\mathbf{k}} \exp(i\mathbf{k} \cdot \mathbf{R}_l) i\omega_{\lambda\mathbf{k}}, \quad (4)$$

where $\omega_{\lambda\mathbf{k}}$ is the phonon frequency. During the simulation, the incident phonon wave packet is generated close to one Si/SiO_2 interface and is then launched towards it as a summation of propagating phonons. When the wave packet reaches the oxide region, scattering events take place; as indicated in Fig. 3, part of the wave packet is transmitted through the SiO_2 layer, while some is reflected back. By determining the energy of each atom, the energy carried by atoms at either side of the SiO_2 layer is determined, from which the energy transmission and reflection coefficients through the interface are determined. The transmission coefficient, α, is the fraction of phonon energy transmitted through the interface, and similarly for the reflection coefficient, α_R. A small part of the energy is trapped in the SiO_2 layer, and slowly dissipates into the Si crystal on either side. At the time at which the analysis is performed, less than 3% of the energy is trapped. When calculating the energy transmission coefficient, this trapped energy is assigned equally to the transmission side and the reflection side. This is a reasonable division since energy that is retained for this extended period is likely to be transmitted or reflected according to the diffuse mismatch model which predicts 50% transmission for this structure.

In order to calculate the Kapitza resistance from phonon scattering at the Si/SiO_2 interface, we sample the first Brillouin Zone (BZ). In particular, the k_x-k_y planes are sampled with an equal spaced mesh scheme (spacing of $0.25 \times 2\pi/a_0$) with the Γ point as the center of the mesh. The k_z direction is meshed with a $0.1 \times 2\pi/a_0$ interval at high k_z, but with a finer mesh close to the Γ point for TA and LA modes. We thus sample at total of 57 crystallographically distinct k-points for the LA mode. Because LO modes have a low group velocity, frequency space is divided into 1 THz intervals for a total of 33 crystallographically distinct k-points. The first BZ sampling grids in all k_x, k_y, and k_z directions are constructed based on the underlying symmetry of the lattice. Because the diamond structure is an FCC lattice with a two-atom basis, the shape of FCC first BZ is a truncated-octahedron. Taking its symmetry into account, we identified 11 irreducible points on $k_z = 0$ plane as the red points shown in Figure 4. The points K and W are not considered, as they are at the corner of the first Brillouin Zone. For simplicity, the points simulated in k_x and k_y from 0 to $2\pi/a$ as integers are labeled 0 and 4. Thus, for example, for the phonons centered at $k_x = 0.25$, $k_y = 0.5$, are labeled as k_{12}.

The total conductance, which is the inverse of resistance, at the SiO_2 junction can be calculated using the equation for an interface conductance by integration over the first BZ[17]

$$\sigma = \frac{1}{(2\pi)^2} \int_{\mathbf{k}} \sum_{\lambda}^{+} \hbar\omega_{\lambda\mathbf{k}} v_{z,\lambda\mathbf{k}} \alpha_{\lambda\mathbf{k}} \frac{dn(\omega, T)}{dT} d\mathbf{k}, \quad (5)$$

where $\alpha_{\mathbf{k}\lambda}$ is the phonon transmission coefficient determined from the PWD simulations for phonon branch λ; ω is the phonon frequency, $\hbar$ is the reduced Planck constant, and n (ω, T) is the Bose-Einstein distribution function at temperature T. The integration over the first BZ is converted to a sum over k-points, with the weighting factor, $W_{\mathbf{k}}$ assigned to each point determined by the associated k-space volume, determined by a Voronoi construction over all the k-points

$$\sigma = \frac{1}{(2\pi)^2} \sum_{\mathbf{k}} \sum_{\lambda}^{+} W_{\mathbf{k}} \hbar\omega_{\lambda\mathbf{k}} v_{z,\lambda\mathbf{k}} \alpha_{\lambda\mathbf{k}} \frac{dn(\omega, T)}{dT}. \quad (6)$$

III. SIMULATION RESULTS

A. Energy transmission coefficient

We start with the sandwich structure which has very thin layer of SiO_2 (0.8 nm in thickness). To develop an

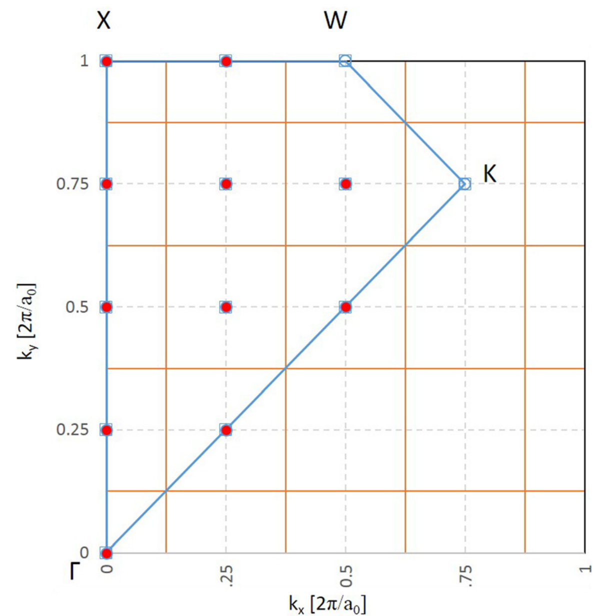

FIG. 4. First Brillouin Zone sampling points in $k_z = 0$ plane. The area delineated by the blue lines is the irreducible region.

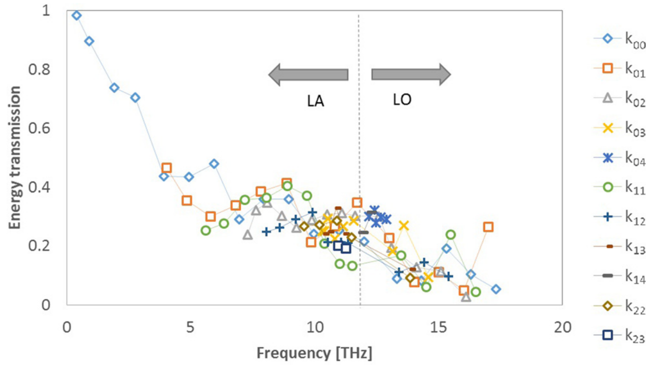

FIG. 5. Transmission coefficients for LA and LO branches as a function of incident phonon frequency. Points on the left of the dashed line belong to the LA branch while those on the right belong to LO branch. Lines are guides to an eye.

understanding of phonon mediated interfacial resistance using the PWD method, we perform simulations with various incident phonon wave-packets for all six branches. Figure 5 shows how the energy transmission coefficients of LA and LO phonons for all available k_{xy} components change as the phonon frequency increases. We note from Figure 5 that there is no qualitative change in the transmission coefficient of the LO modes compared to the LA modes; that is, the transmission coefficient is largely just a function of the frequency regardless of the phonon symmetry. Moreover, we can also see that the transmission coefficient is not strongly sensitive to the phonon branch. This conclusion is reinforced in Figure 6, which shows the energy transmission coefficients of only the k_{00} phonons for all four non-degenerate phonon branches.

Klemens[18] has determined the frequency dependence of phonon scattering probability for various defects structures by using perturbation theory. Within this approach the probability is a power function of the phonon frequency, with the values of the exponent determined by the defect. Thus, we also attempt to fit the reflection coefficient to frequency to a power equation, as following:

$$R(\omega) = a\omega^b, \tag{7}$$

where R is the coefficient of reflection, ω is the phonon frequency, and a and b are coefficients to fit. As shown in Figure 6, we obtain a reasonable good fit with $a = 0.225$ and $b = 0.515$. Klemens' theory[18] predicts $b = 0$ for the ideal grain boundary and $b = 4$ for point defects. Thus, $b = 0.515$ indicates a stronger scattering than an ideal grain boundary, which we attribute to the disorder in the SiO_2 layer.

We also vary the SiO_2 layer thickness to determine the energy transmission coefficients. The energy transmission is further decreased with increased thickness of the SiO_2 layer: as shown in Figure 7, there is uniform decrease in energy transmission as the SiO_2 layer becomes thicker ($l_{SiO2} = 0.8$ nm to $l_{SiO2} = 10.9$ nm). We will return to the effect of thickness in Sec. III D.

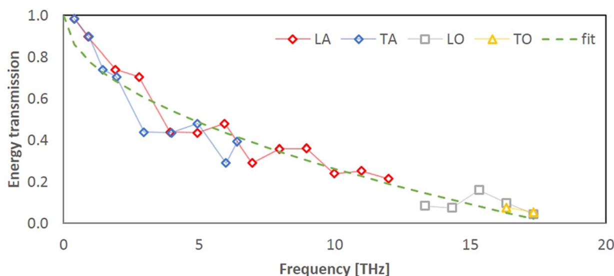

FIG. 6. Transmission coefficients for all modes along k_{00} direction for $l_{sio2} = 0.8$ nm structure. The dashed line is the fit discussed in the text.

B. Phonon scattering

The phonon launched at the SiO_2 region are vibrational modes of the Si lattice. Thus, scattering can only take place at the interface and in the SiO_2 block which has different vibrational properties. Consequently, when the wave packet frequency is low, i.e., its wavelength is larger than the space dimensions of most defects, the phonon can easily travel through the SiO_2 region with very little reflection. A simple calculation shows that a wavelength equal to the SiO_2 layer thickness of 0.8 nm corresponds to a frequency of ~10 THz. When the wavevector approaches the Γ point (the first point of k_{00} line in Figure 5), the transmission coefficient approaches unity; for these long wavelengths, the relatively narrow SiO_2 regions do not present a significant obstacle to the phonon waves. However, as the incident phonon frequency increases, its wavelength becomes more and more comparable with the dimensions of the defected region, yielding more intense phonon scatterings. This can be seen in Figure 8, which shows how the transmitted phonon energy of initially pure k_{00} phonons scatters into various k_{xy} points. As we can see, as the incident frequency increases, the transmitted energy distribution in k_{xy} is more widely spread. For instance, in the $f = 8$ THz case, we no longer see the dominant energy share in k_{00}. To better quantify this dispersion statistically, we introduced a weighted wavevector deviation (d_k) as defined in Eq. (8)

$$d_k = \sqrt{\frac{\sum_n |\mathbf{k}_n - \mathbf{k}_0|^2 E_n}{\sum_n E_n}}, \tag{8}$$

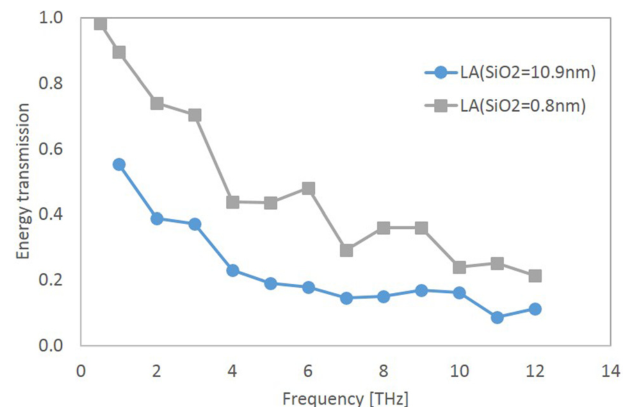

FIG. 7. LA incident phonon transmission for $l_{SiO2} = 0.8$ nm (squares) and $l_{SiO2} = 10.9$ nm (circles).

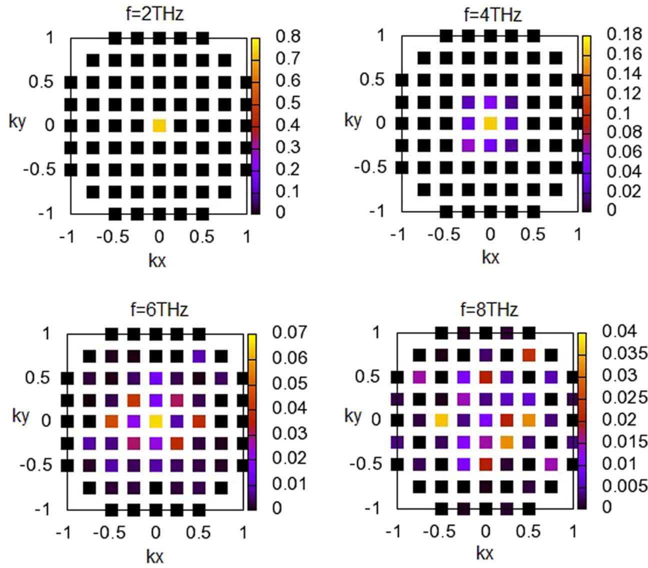

FIG. 8. Relative transmitted energy as a function of k_x and k_y for four different incident phonon frequencies. All shown are for k_{00} LA incident phonon on $l_{SiO2} = 0.8$ nm. Note that the scales are different in each figure and all kx and ky have the unit of $2\pi/a_0$.

where $\mathbf{k}_0$ is the peak of the incident phonon wavevector, $\mathbf{k}_n$ and E_n are the transmitted/reflected phonon wavevector and associated energy, respectively, and the summation is over all the available phonon wavevector for the transmission or reflection phonons. d_k essentially measures how much the average phonon momentum deviates from its initial value. The larger the deviation, the less character of the initial phonon features is preserved. We plot d_k as a function of incident phonon frequency in Figure 9. Clearly scattering increases with increasing frequency causing that scattered phonons to lose forward momentum. The rest of the momentum is scattered to the non-normal directions as shown in Figure 8. There is also less energy transmitted as the phonons lose forward momentum, and more energy is reflected back. As a consequence there is a decrease in energy transmission with increasing frequency.

C. Phonon mode conversion

In addition to scattering into different directions, we have also observed phonon mode conversion after the

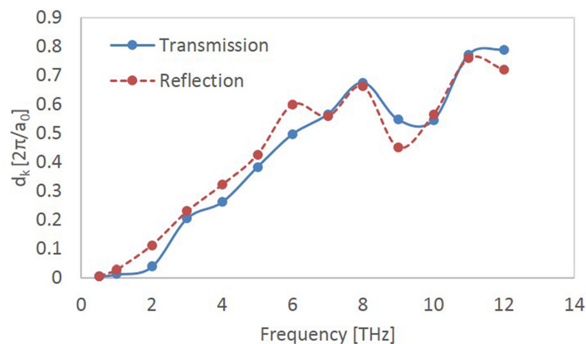

FIG. 9. Wavevector deviation as a function of incident phonon frequency for transmission and reflection phonons for $l_{SiO2} = 0.8$ nm structure, only LA data are shown.

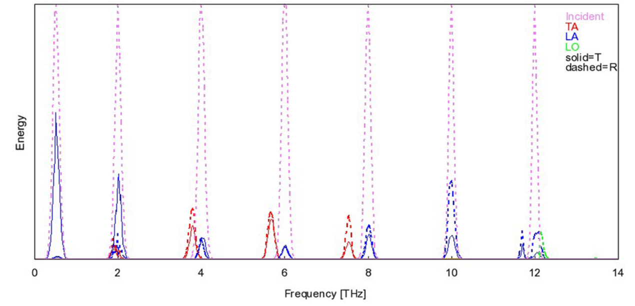

FIG. 10. Frequency distribution of wave packets for $l_{SiO2} = 0.8$ nm structure. All incident phonons are in pure k_{00} LA modes. All energies shown are relative and scaled to the same incident energy.

scattering at the interface. Figure 10 shows the phonon wave packet energy partition into various phonon modes as a function of incident LA phonon energies. The pink dotted lines indicate the initially pure LA phonon wave packet energy distribution for various incident phonon frequencies. The blue lines and red lines are the energy distributions of LA and TA modes, with dashed lines indicating reflection and solid lines indicating transmission. We can clearly see the energy shift (peak shift between blue and red) and mode conversion (phonon modes other than blue) as the incident phonon frequency increases; the LA-TA conversion cannot take place at high frequency as there are no TA modes available. It is interesting that the LA modes still maintain their original frequency but the frequency of the converted TA modes gradually shifts away from the incident phonon frequency indicating more intense scattering events. Such phonon mode conversion is known to take place when phonons interact with interfaces,[19,20] a result of anharmonic phonon scattering at the interface.[21] This indicates that as phonon frequency increases (in the region that TA modes are still available), phonon mode conversion also increases, thereby increasing the energy transmission coefficient. Thus, this provides evidence that anharmonic scatterings open up additional channels for phonon transmission thus reducing interfacial thermal resistance at high frequencies.[22,23]

D. Kapitza resistance

The energy transmission coefficients for individual modes alone are not sufficient to enable the Kapitza resistance to be determined. Thus, we calculate the Kapitza resistance using Eq. (6) as described previously. Since the factor W(k) in Eq. (6) is the volume weighting factor of the First Brillouin Zone, and the mesh grid in k_{xy} plane is equally spaced, we rewrite the factor as $W(\mathbf{k}) = W_{xy}(\Delta k_x, \Delta k_y) W_z(\Delta k_z)$. By first summing up the W_z only, we obtain the relative contribution to the conductance at each (k_x, k_y), as shown in Figure 11. Clearly, as k_x or k_y increases, under the same frequency, their relative conductance drops rapidly because the k_z component of the wave vector decreases. Although Figure 5 shows that all non-perpendicular incident phonons have similar energy transmission coefficients, their contributions to the conductance can be different due to their different phonon group velocities and available k_z dimension in the First Brillouin Zone.

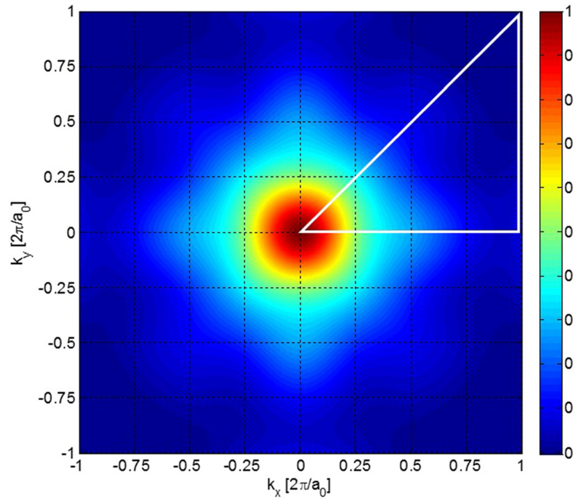

FIG. 11. Contribution to the thermal conductivity as a function of k_x and k_y, with summation of all k_z contribution. Data are fit by interpolation and line integration at each (k_x, k_y). The region inside the white triangle indicates the region of the calculation, while the rest is plotted by exploiting the symmetry of the first Brillouin Zone.

As discussed above, our system consists of two Si/SiO_2 interfaces and the slightly strained β-cristobalite SiO_2 bulk. The total resistance ($1/\sigma_T$) in our system should be[4]

$$\frac{1}{\sigma_T} = \frac{2}{\sigma_K} + \frac{l_{SiO_2}}{k_{SiO_2}},$$

where $1/\sigma_T$ is the total resistance from simulation, $1/\sigma_K$ is the Kapitza resistance of Si/SiO_2 interface, the factor of 2 indicates the two interfaces, $1/k_{SiO2}$ is the thermal resistivity of SiO_2, and l_{SiO2} is the length of the silica layer. To determine the pure Kapitza resistance of Si/SiO_2 that we are interested in, we varied the silica layer thickness l_{SiO2} and calculated the total resistance. By performing a linear extrapolation according to Eq. (3), at $l_{Sio2} = 0$ we obtain the Kapitza resistance of the individual interface. We perform the calculation using both NEMD and PWD methods. For the PWD method, we only performed the full First Brillouin Zone sampling for the $l_{SiO2} = 0.8$ nm and $l_{SiO2} = 2.2$ nm structure. We have calculated the relative contribution to total resistance from k_{00} of both structure and confirmed that its contribution is almost the same for the two structures. Therefore, for the other thicknesses of SiO_2 layer, we only sampled the k_{00} direction and scaled the results with the same contribution from $l_{sio2} = 0.8$ nm k_{00} data. This is justified by the dominant contribution of k_{00} to the total conductance as shown in Figure 11. The NEMD simulation is performed at 300 K, and by utilizing the Bose-Einstein phonon distribution function (Eq. (5)), we were also able to calculate the Kapitza resistance at 300 K using PWD method. Figure 12 shows the thermal conductivity as a function of thickness of the SiO_2 layer as determined from the NEMD and PWD methods. The Si/SiO_2 Kapitza resistance, determined from the intercepts, is $1.48(\pm 0.46) \times 10^{-9}$ m^2K/W from NEMD and is $1.37(\pm 0.42) \times 10^{-9}$ m^2K/W from PWD. The good agreement of the results from PWD and NEMD methods suggests that they have captured the same physics

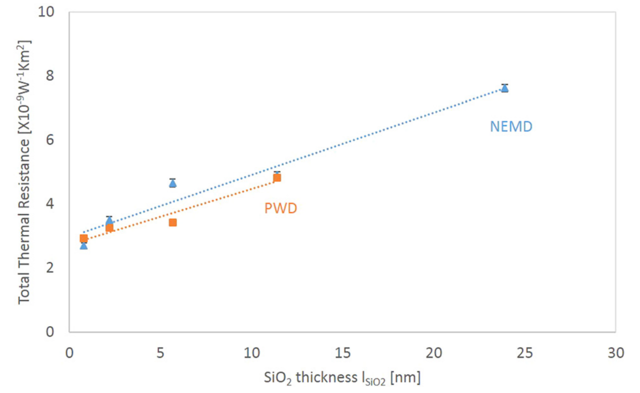

FIG. 12. Extracting the Kapitza resistance of the Si/SiO_2 interface at 300 K. The extrapolated values at $l_{SiO2} = 0$ are 2.96×10^{-9} and 2.74×10^{-9} m^2K/W for NEMD and PWD, respectively, which are twice the Kapitza resistance obtained from Eq. (4).

of the interfacial thermal phonon scattering, discussed in Sec. III B. The relatively large error bars here are due to the linear regression since we only have a small number of data points. We also use the power-law fit in Sec. III A to calculate the Kapitza resistance, giving us $1.83(\pm 0.09) \times 10^{-9}$ m^2KW^{-1}. Although the value is not exactly the same from our atomistic method, it has provided a more convenient way to estimate the Kapitza resistance.

The experiments by Hurley *et al.*[2] mentioned in the first section, measured the Kapitza resistance to be 2.3×10^{-9} m^2KW^{-1} as an upper limit by considering all sources of uncertainties. Comparing with the multi-magnitude measurements from experiments,[4] our results remain in the same magnitude. And in particular, the atomistic model we used has a one-to-one correspondence with the experiment settings, thus, the comparison is more reliable. However, we do note that, as a classical simulation, the potential we used will have an effect on the final values.

In addition to the overall value, the PWD also provides a mode-by-mode contribution to the thermal conductivity.

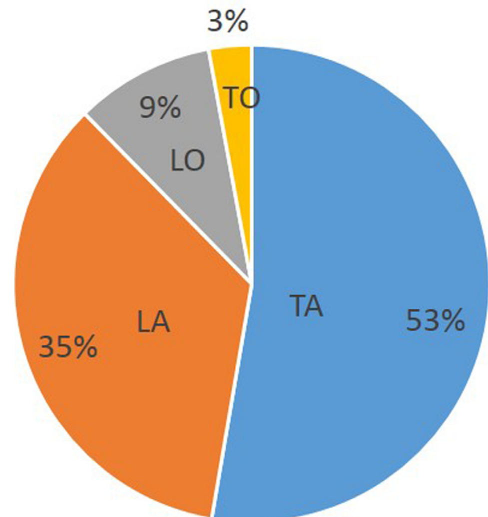

FIG. 13. Contribution to Kapitza conductance by mode for $l_{SiO2} = 0.8$ nm. Both TA and TO include the contribution of two transverse modes. The mode-wise contribution is almost the same for $l_{SiO2} = 2.2$ nm structure.

Using Fourier analysis, we find the mode-wise contribution to Kapitza conductance in Figure 13. The acoustic modes contribute 88% to the total Kapitza conductance, while the optical modes contribute only 12%. This agrees with the conventional understanding that the acoustic phonons are the main heat carriers in silicon.[24]

IV. CONCLUSIONS

We have investigated Si/SiO_2/Si sandwich structure by PWD and NEMD approaches. These methods provide similar values for the Si/SiO_2 Kapitza resistance; this value is also consistent with the experimental results. We have demonstrated that PWD approach provides far more detailed information about thermal transport through the interface. In particular, for the system of interest here we found that the acoustic phonons are the main contributor to the conductance through the interface. The phonon anharmonic scattering provides additional channels for phonon transport. We have also analyzed the phonon energy transmission at the interface using PWD. Frequency dependence of the reflection coefficient was found to be stronger ($f \sim \omega^{0.5}$) than predicted by Klemens' theory for the ideal planar defect ($\sim\omega^0$). We associated this with the disordered nature of the studied interface. The fact that transmission coefficient is fitted very well by a power law can be used in the mesoscale models of the phonon transport.[25] We do note that in some amorphous systems, the fractal geometry could affect the thermal transport.[26] However, the correlation length[27] of the SiO_2 layer should be very small compared to our structure dimension. Thus, the SiO_2 layer in our simulation is dynamically homogeneous and the fractal geometry should not affect our results.

ACKNOWLEDGMENTS

This work was supported by the U.S. Government under DOE Contract No. DE-AC07-05ID14517, under the Energy Frontier Research Center (Office of Science, Office of Basic Energy Science, FWP 1356). Accordingly, the U.S. Government retains and the publisher (by accepting the article for publication) acknowledges that the U.S. Government retains a nonexclusive, paid-up, irrevocable, world-wide license to publish or reproduce the published form of this manuscript, or allow others to do so, for U.S. Government purposes.

[1] G. K. Celler and S. Cristoloveanu, J. Appl. Phys. **93**, 4955 (2003).
[2] D. H. Hurley, M. Khafizov, and S. L. Shinde, J. Appl. Phys. **109**, 083504 (2011).
[3] S. S. Mahajan, G. Subbarayan, and B. G. Sammakia, "Estimating Kapitza resistance between Si-SiO2 interface using molecular dynamics simulations," in *Thermal and Thermomechanical Phenomena in Electronic Systems* (2008), p. 1055.
[4] E. Lampin, Q. H. Nguyen, P. A. Francioso, and F. Cleri, Appl. Phys. Lett. **100**, 131906 (2012).
[5] S. Munetoh, T. Motooka, K. Moriguchi, and A. Shintani, Comput. Mater. Sci. **39**, 334 (2007).
[6] J. Chen, G. Zhang, and B. W. Li, J. Appl. Phys. **112**, 064319 (2012).
[7] M. Yao, T. Watanabe, P. K. Schelling, P. Keblinski, D. G. Cahill, and S. R. Phillpot, J. Appl. Phys. **104**, 024905 (2008).
[8] P. K. Schelling, S. R. Phillpot, and P. Keblinski, Appl. Phys. Lett. **80**, 2484 (2002).
[9] P. K. Schelling, S. R. Phillpot, and P. Keblinski, J. Appl. Phys. **95**, 6082 (2004).
[10] T. Watanabe, H. Fujiwara, H. Noguchi, T. Hoshino, and I. Ohdomari, Jpn. J. Appl. Phys., Part 2 **38**, L366 (1999).
[11] T. Watanabe and I. Ohdomari, Thin Solid Films **343–344**, 370 (1999).
[12] T. Watanabe, K. Tatsumura, and I. Ohdomari, Appl. Surf. Sci. **237**, 125 (2004).
[13] F. H. Stillinger and T. A. Weber, Phys. Rev. B: Condens. Matter **31**, 5262 (1985).
[14] D. A. Broido, A. Ward, and N. Mingo, Phys. Rev. B **72**, 014308 (2005).
[15] J. D. Gale, J. Chem. Soc., Faraday Trans. **93**, 629 (1997).
[16] G. Dolling, *Inelastic Scattering Neutrons in Solids and Liquids* (International Atomic Energy Agency, Unesco, 1963), p. 37.
[17] C. Kimmer, S. Aubry, A. Skye, and P. K. Schelling, Phys. Rev. B **75**, 144105 (2007).
[18] P. G. Klemens, Solid State Phys.-Adv. Res. Appl. **7**, 1–98 (1958).
[19] X. B. Li and R. G. Yang, Phys. Rev. B **86**, 054305 (2012).
[20] G. Chen, T. Zeng, T. Borca-Tasciuc, and D. Song, Mater. Sci. Eng., A **292**, 155 (2000).
[21] J. Wang and J. S. Wang, J. Appl. Phys. **105**, 063509 (2009).
[22] Y. Z. Ge and S. G. Chen, Solid State Commun. **77**, 313 (1991).
[23] M. Hu, P. Keblinski, and P. K. Schelling, Phys. Rev. B **79**, 104305 (2009).
[24] S. Mazumder and A. Majumdar, J. Heat Transfer **123**, 749 (2001).
[25] A. J. H. McGaughey and A. Jain, Appl. Phys. Lett. **100**, 061911 (2012).
[26] J. K. Kjems, Phys. A **191**, 328 (1992).
[27] M. I. Ojovan, J. Non-Cryst. Solids **382**, 79 (2013).